Effective magnetic moment of magnetic multicore nanoparticles

Vincent Schaller,[1],[*] Göran Wahnström,[2] Anke Sanz-Velasco,[1] Stefan Gustafsson,[2] Eva Olsson,[2]
Peter Enoksson,[1] and Christer Johansson[3]

[1]*Department of Microtechnology and Nanoscience - MC2, Chalmers University of Technology, SE-412 96 Göteborg, Sweden*
[2]*Department of Applied Physics, Chalmers University of Technology, SE-412 96 Göteborg, Sweden*
[3]*Imego Institute, Arvid Hedvalls Backe 4, P.O. Box 53071, SE-400 14 Göteborg, Sweden*
(Received 3 July 2009; published 22 September 2009)

We carry out Monte Carlo simulations to study the effective magnetic moment μ_{eff} in the low-field region of magnetic multicore nanoparticles. Transmission electron microscopy and scanning electron microscopy images show that these particles contain a number of magnetic nanocrystals (MNCs) randomly packed in a single cluster of total volume V_{tot}. We illustrate how the initial magnetic susceptibility χ_0 of magnetic multicore nanoparticles can be straightforward derived from μ_{eff} computed at zero magnetic field. We observe that dipolar interactions between MNCs and polydispersity of the MNCs contribute to increase and to decrease $\mu_{\mathrm{eff}}/V_{\mathrm{tot}}$, respectively, while magnetic anisotropy of the MNCs does not show any effect. In all three cases, $\mu_{\mathrm{eff}}/V_{\mathrm{tot}}$ can be described by a linear relation to $(\mu B/k_B T)^2$ that we analytically derived for low applied fields.

I. INTRODUCTION

In recent years, there has been growing interest in using magnetic multicore nanoparticles in biomedical applications such as magnetic carriers in bioseparation[1–3] and drug delivery,[4,5] mediators for hyperthermia in cancer treatment,[6–8] contrast agents for magnetic resonance imaging,[5,9] and magnetic probes for biosensing.[10–14] These particles have a hydrodynamic diameter of typically 50–200 nm and contain a cluster of magnetic nanocrystals (MNCs) surrounded by a polymer or organic coating (e.g., dextran and starch) that can be functionalized with target-specific biomolecules such as antibodies, DNA, and peptides.

A large number of biosensing systems using magnetic multicore nanoparticles as markers rely on the magnetic response of these particles in the low-field region, i.e. in the mT range[12,14] or below.[10,11,13] Consequently, it is essential to understand how the magnetic properties and physical microstructure of the MNC cluster influence the magnetic response of the particles to optimize the choice of particles and to guarantee proper interpretation of the experimental data. Although considerable work has been devoted to single-core nanoparticles,[15–20] little attention has been paid to multicore nanoparticles yet.

In this paper, we investigate the effective magnetic moment of magnetic multicore nanoparticles at zero and low applied magnetic fields using a Monte Carlo (MC) method.[21] Our model takes into account (i) the specific microstructure of the MNC cluster as observed from scanning and transmission electron microscopy (SEM and TEM) images of commercially available multicore nanoparticles, (ii) the size distribution and (iii) magnetic anisotropy of the MNCs, (iv) the magnetic dipole-dipole interactions between the MNCs, and (v) the Brownian stochastic rotation of the particle suspended in liquid.

II. MODEL AND METHOD

SEM and TEM images of typical magnetic multicore nanoparticles are shown in Figs. 1(a) and 1(b), respectively.

Specimens for SEM and TEM were prepared by placing a drop of the ferrofluid on a standard Cu grid coated with a holey carbon film. The particles were imaged using a Leo Ultra 55 SEM and a Philips CM200 TEM operating at 10 and 200 kV, respectively. We observe that each multicore nanoparticle contains a single cluster of randomly packed MNCs that have a nearly spherical shape and a certain size distribution well described by a log-normal distribution function.

The first step of the simulation is to generate a three-dimensional (3D) cluster of N spheres representing the MNCs within the multicore nanoparticle. The ith spherical MNC has a diameter D_i randomly chosen from a log-normal function with mean diameter D_m and distribution parameter σ. After the first MNC is placed at the origin of the coordinate system, the cluster is *grown* by successively adding a new MNC with index $i=[2:N]$ to the contact of a randomly chosen MNC with index $j < i$. The center of the new MNC is located at a distance $D_i + D_j$ from the center of the jth MNC and with random direction in 3D, excluded positions that would result in an overlap with other MNCs already present in the cluster. It should be noted that the method proposed here is obviously not intended to reproduce the complex and often not fully understood mechanisms behind the aggregation and growth of real MNC clusters. Nevertheless, we ob-
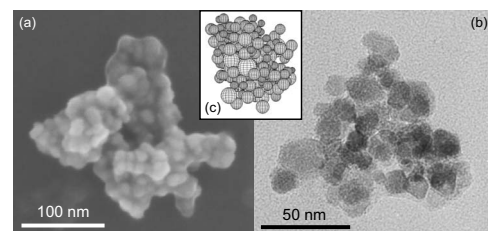

FIG. 1. (a) Scanning and (b) transmission electron microscopy images of magnetic multicore nanoparticles fluidMAG-D150 from Chemicell GmbH (average hydrodynamic diameters of about 150 nm). The magnetic multicore consists of a cluster of many MNCs of magnetite (Fe_3O_4) with mean diameters of about 12 nm embedded in a starch coating. (c) Simulated 3D cluster of $N=200$ MNCs with mean diameters $D_m=12$ nm and $\sigma=3$ nm.

serve that this rather simple approach produces clusters that have all the essential microstructural features of real particle systems [Fig. 1(c)].

The equilibrium magnetization of the MNCs is then simulated using the same standard Metropolis algorithm as reported in Ref. 22. In brief, we assume that each MNC is homogeneously magnetized due to the coherent rotation of the atomic moments within the MNC.[23] The magnetic moment of the ith MNC is represented by a dipole $\boldsymbol{\mu}_i$ located at the center of the MNC with constant magnitude $\mu = M_S V_i$, where M_s is the intrinsic saturation magnetization and $V_i = (\pi/6)D_i^3$ is the volume of the ith MNC, respectively.

The interaction energy between $\boldsymbol{\mu}_i$ and the applied magnetic field $\mathbf{B}$ is given by

$$E_B^{(i)} = -\boldsymbol{\mu}_i \cdot \mathbf{B}. \tag{1}$$

The magnetic dipole-dipole interaction energy between $\boldsymbol{\mu}_i$ and its neighbors $\boldsymbol{\mu}_j$ is expressed as

$$E_D^{(i)} = -\frac{\mu_0}{4\pi} \sum_{j \neq i} \left[\frac{3(\boldsymbol{\mu}_i \cdot \mathbf{r}_{ij})(\boldsymbol{\mu}_j \cdot \mathbf{r}_{ij})}{r_{ij}^5} - \frac{(\boldsymbol{\mu}_i \cdot \boldsymbol{\mu}_j)}{r_{ij}^3} \right], \tag{2}$$

where $\mu_0 = 4\pi \times 10^{-7}$ N/A^2 is the vacuum permeability and $\mathbf{r}_{ij} = \mathbf{r}_i - \mathbf{r}_j$ is a distance vector joining the two dipoles ($r_{ij} = \|\mathbf{r}_{ij}\|$). Owing to the small and finite size of the system, all neighbor pairs are considered in the summation of Eq. (2).

The uniaxial magnetic anisotropy energy is represented by

$$E_A^{(i)} = -K_u V_i \left(\frac{\boldsymbol{\mu}_i}{|\boldsymbol{\mu}_i|} \cdot \mathbf{e}_i \right)^2, \tag{3}$$

where K_u is the anisotropy constant and $\mathbf{e}_i$ is a unit vector along the randomly distributed easy axis of each MNC.

Adding Eqs. (1)–(3), the total energy of the ith MNC becomes

$$E_{\text{tot}}^{(i)} = E_B^{(i)} + E_D^{(i)} + E_A^{(i)}. \tag{4}$$

At each Monte Carlo step, a new direction of $\boldsymbol{\mu}_i$ is randomly chosen with a uniform distribution in all directions. The move is accepted or rejected according to the Metropolis criterion[21] with the probability determined by the Boltzmann distribution factor, i.e., $\exp(-\Delta E_{\text{tot}}^{(i)}/k_B T)$, where $k_B T$ is the thermal energy and $\Delta E_{\text{tot}}^{(i)}$ is the energy difference between the new and current magnetization orientations calculated from Eq. (4).

The total magnetic moment of the particle, μ_{tot}, is then calculated as the Euclidian vector norm of the vector sum of the N individual dipoles $\boldsymbol{\mu}_i$,

$$\mu_{\text{tot}} = \left\| \sum_{i=1}^{N} \boldsymbol{\mu}_i \right\|. \tag{5}$$

Finally, we define the effective magnetic moment of the particle, μ_{eff}, as the root mean square of μ_{tot},

$$\mu_{\text{eff}} = \langle \mu_{\text{tot}}^2 \rangle_n^{1/2}, \tag{6}$$

where the symbol $\langle \ \rangle_n$ denotes the average value over n MC steps after the system has reached thermal equilibrium.

The initial magnetic susceptibility χ_0 is often determined from the initial slope of the magnetization curve, i.e., χ_0 $= \partial M / \partial H_{(H \to 0)}$, thus requiring a number of magnetization values calculated in the low-field region.[24] Instead, χ_0 can be straightforward derived in a single step from μ_{eff} computed at zero applied field,

$$\chi_0 = \mu_0 \frac{1}{V_{\text{tot}}} \frac{\mu_{\text{eff}}^2}{3 k_B T}, \tag{7}$$

where V_{tot} is the total volume of all the MNCs contained in the cluster. It is worth to note that this value of χ_0 directly includes the effect of size distribution and magnetic anisotropy of the MNCs, and dipole-dipole interactions between the MNCs.

In order to compare the effect of these contributions in the low-field region, we derived an analytical expression of μ_{eff} for an ensemble of N noninteracting monodisperse MNCs with magnetic moments μ,

$$\mu_{\text{eff}} = \sqrt{N \mu^2 \left[1 + \frac{(N-1)}{2} \left(\frac{\mu B}{3 k_B T} \right)^2 \right]}. \tag{8}$$

This equation was obtained under the condition $(N-1)(\mu B/3 k_B T)^2 \ll 1$, which is fulfilled in our case with $N = 100$. At zero magnetic field, Eq. (8) reduces to

$$\mu_{\text{eff}} = \sqrt{N} \mu = \sqrt{N} M_S V. \tag{9}$$

All the simulations were performed at $T = 293$ K and with parameter values $M_s = 350$ kA/m and $K_u = 50$ kJ/m^3, which are typical values for MNCs of magnetite (Fe$_3$O$_4$).[25,26] All the simulated clusters contain $N = 100$ MNCs, which corresponds to the typical number of MNCs contained in magnetic multicore nanoparticles with an intermediate size of about 100 nm. The initial 5000 MC steps were performed to let the system reach thermal equilibrium. Then the data were collected during the following 15 000 MC steps. The simulation is repeated 64 times at every field with a new cluster created each time.

III. RESULTS AND DISCUSSION

The results hereafter are presented for particles including one or several of the following factors: (I) particle rotation in the liquid and interaction with the external field (if any); (II) uniaxial magnetic anisotropy of the MNCs; (III) log-normal size distribution of the MNCs (with mean diameter D_m and standard deviation σ); (IV) dipole-dipole interactions between the MNCs.

Figures 2 and 3 illustrates $\mu_{\text{eff}}/V_{\text{tot}}$ vs $(\mu B/k_B T)^2$ in the low-field region where, according to Eq. (8), $\mu_{\text{eff}}/V_{\text{tot}}$ can be approximated by a linear relation to $(\mu B/k_B T)^2$,

$$\frac{\mu_{\text{eff}}}{V_{\text{tot}}} = A_0 + A_2 \left(\frac{\mu B}{k_B T} \right)^2, \tag{10}$$

In the Langevin model, the parameters A_0 and A_2 are given by
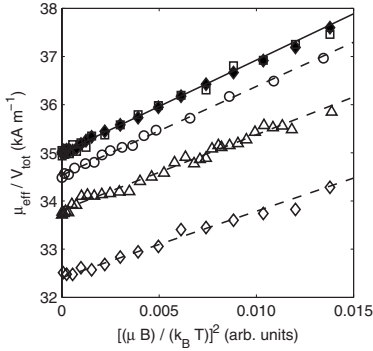
$$A_0 = \frac{M_S}{\sqrt{N}},$$

FIG. 2. Simulated values of $\mu_{\text{eff}}/V_{\text{tot}}$ vs $(\mu B/k_B T)^2$ for particles type I (filled diamonds), type I+II (open squares), and type I+IV (open circles: $D=8$ nm, open triangles: $D=10$ nm, and open diamonds: $D=12$ nm). The analytical expression derived for particles type I, Eq. (8), is plotted as a solid line. The dashed lines represent Eq. (10) fitted to the simulation data for the three different MNC diameters.

$$A_2 = \frac{(N-1)}{18} A_0. \tag{11}$$

It is noteworthy that parameters A_0 and A_2 are linearly proportional and independent of both the MNC size and the temperature. Parameter A_0 gives the zero-field value of the effective magnetic moment, which directly relates to the initial magnetic susceptibility χ_0 of the multicore particle as described in Eq. (7). Parameter A_2 relates to the third harmonic of the particle's magnetic response and therefore this parameter is of particular interest for applications taking advantage of the nonlinear magnetic response of magnetic nanoparticles such as tomographic imaging[27] and biosensing.[28,29]

A linear interpolation was performed for each series of data and the corresponding fitting parameters A_0 and A_2 are summarized in Table I. The Langevin model predicts values $A_0=35.0$ kA/m and $A_2=192.5$ kA/m for $M_S=350$ kA/m and $N=100$ [Eq. (11)].

Simulations with particles type I were carried out for several MNC diameters. All data superimposed onto a universal curve of $\mu_{\text{eff}}/V_{\text{tot}}$ vs $(\mu B/k_B T)^2$ with both parameters A_0 and A_2 recovering the values predicted by the Langevin model (only the data for $D=12$ nm are represented in Fig. 2 for the sake of visibility).

Similarly, simulated values for particles type I+II (open squares in Fig. 2) show no significant deviation from the analytical expression, indicating that magnetic anisotropy with randomly distributed easy axes does not influence μ_{eff} in the low-field region, which is in agreement with previous work.[19,30]

On the other hand, dipolar interactions (particles type I+IV) yield a decrease in μ_{eff} compared to the noninteracting case. This result agrees with a previous study by Chantrell *et al.*[15,16] where a reduction in χ_0 for an ensemble of single-core nanoparticles was attributed to the formation of flux-closure configurations due to interparticle dipolar interactions. Although the largest packing density (0.35) of the single-domain particles in Ref. 16 is below the correspond-
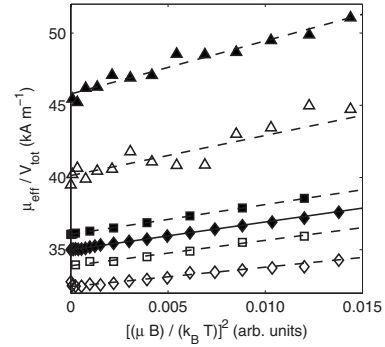

FIG. 3. Simulated values of $\mu_{\text{eff}}/V_{\text{tot}}$ vs $(\mu B/k_B T)^2$ for particles type I (filled diamonds), type I+III (filled squares: $D_m=12$ nm and $\sigma=1$ nm, filled triangles: $D_m=12$ nm and $\sigma=3$ nm), type I+IV (open diamonds), and type I+III+IV (open squares: $D_m=12$ nm and $\sigma=1$ nm, open triangles: $D_m=12$ nm and $\sigma=3$ nm). The analytical expression derived for particles type I, Eq. (8), is plotted as a solid line. The dashed lines represent Eq. (10) fitted to the different series of simulated data.

ing value for typical multicore nanoparticles (about 0.5 which corresponds to a typical concentration of magnetic material of 70 wt %), it is reasonable to assume that the same phenomenological explanation applies in the case multicore nanoparticles. Interestingly, the values $\mu_{\text{eff}}/V_{\text{tot}}$ for particles type I+IV with $D=8$, 10, and 12 nm (open circles, triangles, and diamonds in Fig. 2) can still be described by Eq. (10).

As can be seen in Table I, the parameter A_0 decreases for larger MNC size. In other words, larger MNCs inducing stronger dipole-dipole interactions have a lower effective magnetic moment per unit volume at zero magnetic field and thus a lower initial magnetic susceptibility χ_0. Consequently, for a given amount of magnetic material within the multicore particle, χ_0 can be optimized by eventually synthesizing MNCs with smaller dimensions. We also note that the parameter A_2 decreases as D increases. This suggests that, as the MNC size increases, the internal field induced by the dipole-dipole interactions more strongly opposes the reorientation of the magnetic moments μ_i caused by the externally applied field.

The effect of the size distribution of the MNCs is depicted in Fig. 3 for particles type I+III and I+III+IV. In both cases,

TABLE I. Parameters A_0 and A_2 for the different series of simulation data illustrated in Figs. 2 and 3.

Particle type	A_0 (kA/m)	A_2 (kA/m)
I($D=12$ nm)	35.0	192.5
I+II($D=12$ nm)	35.0	183.6
I+III($D_m=12$ nm, $\sigma=1$ nm)	36.1	205.2
I+III($D_m=12$ nm, $\sigma=3$ nm)	45.8	367.2
I+IV($D=8$ nm)	34.5	184.0
I+IV($D=10$ nm)	33.8	156.3
I+IV($D=12$ nm)	32.5	135.0
I+III+IV($D_m=12$ nm, $\sigma=1$ nm)	33.9	176.2
I+III+IV($D_m=12$ nm, $\sigma=3$ nm)	40.1	277.8

the simulated values of $\mu_{\text{eff}}/V_{\text{tot}}$ obey Eq. (10). For polydisperse MNCs, we use $\mu = M_S\langle V\rangle$. The average volume of the MNC ensemble, $\langle V\rangle$, is calculated as

$$\langle V\rangle = \frac{\pi}{6}\int_{D_{\min}}^{D_{\max}} D^3 f(D)dD, \qquad (12)$$

where $D_{\min}$ and $D_{\max}$ are the minimum and maximum diameters of the MNC ensemble, respectively, and $f(D)$ is a log-normal function with parameters D_m and σ.

As expected from Eqs. (9) and (12), the size distribution of the MNCs [particles type I+III with $\sigma=1$ (filled squares) and $\sigma=3$ nm (filled triangles)] yields an increase in $\mu_{\text{eff}}/V_{\text{tot}}$ compared to monodisperse MNCs (filled diamonds).

While the size distribution of the MNCs contribute to increase $\mu_{\text{eff}}/V_{\text{tot}}$, dipolar interactions between MNCs yield a decrease in this parameter value. Consequently, the values of $\mu_{\text{eff}}/V_{\text{tot}}$ for particles type I+III+IV are the result of the interplay between these two contributions. This may result in either lower or higher values of $\mu_{\text{eff}}/V_{\text{tot}}$ (open squares and triangles, respectively) compared to the reference curve for

particles type I (solid line), depending on the size-distribution parameter σ.

IV. CONCLUSIONS

Monte Carlo simulations of magnetic multicore nanoparticles in thermal equilibrium have shown that in the low-field region $\mu_{\text{eff}}/V_{\text{tot}}$ is reduced owing to the dipole-dipole interactions between MNCs whereas the size distribution of the MNCs yield a higher value of $\mu_{\text{eff}}/V_{\text{tot}}$. Uniaxial magnetic anisotropy of the MNCs with randomly distributed easy axes does not influence μ_{eff} at zero field. We have shown how the true value of χ_0 can be straightforward derived from the effective μ_{eff} computed at zero field. We also derived a linear relation of μ_{eff} to $(\mu B/k_B T)^2$. The fitting parameters relate directly to χ_0 and to the nonlinearity of the particle's magnetic response. These findings are expected to be of particular interest for biomedical applications relying on either the linear or the nonlinear magnetic response of magnetic multicore nanoparticles.

*Author to whom correspondence should be addressed. FAX: +46-31-772 3622; vincent.schaller@chalmers.se

[1] S. Sieben, C. Bergemann, A. Lübbe, B. Brockmann, and D. Rescheleit, J. Magn. Magn. Mater. **225**, 175 (2001).

[2] N. L. Adolphi, D. L. Huber, J. E. Jaetao, H. C. Bryant, D. M. Lovato, D. L. Fegan, V. L. Venturini, T. C. Monson, T. E. Tessier, H. J. Hathaway, C. Bergemann, R. S. Larson, and E. R. Flynn, J. Magn. Magn. Mater. **321**, 1459 (2009).

[3] V. Schaller, U. Kräling, C. Rusu, K. Petersson, J. Wipenmyr, A. Krozer, G. Wahnström, A. Sanz-Velasco, P. Enoksson, and C. Johansson, J. Appl. Phys. **104**, 093918 (2008).

[4] U. Steinfeld, C. Pauli, N. Kaltz, C. Bergemann, and H.-H. Lee, Int. J. Pharm. **311**, 229 (2006).

[5] J. Yang, C.-H. Lee, J. Park, S. Seo, E.-K. Lim, Y. J. Song, J.-S. Suh, H.-G. Yoon, Y.-M. Huh, and S. Haam, J. Mater. Chem. **17**, 2695 (2007).

[6] M. Kettering, J. Winter, M. Zeisberger, S. Bremer-Streck, H. Oehring, C. Bergemann, C. Alexiou, R. Hergt, and K. Halbhuber, Nanotechnology **18**, 175101 (2007).

[7] S. Dutz, J. H. Clement, D. Eberbeck, T. Gelbrich, R. Hergt, R. Muller, J. Wotschadio, and M. Zeisberger, J. Magn. Magn. Mater. **321**, 1501 (2009).

[8] M. Kallumadil, M. Tada, T. Nakagawa, M. Abe, P. Southern, and Q. A. Pankhurst, J. Magn. Magn. Mater. **321**, 1509 (2009).

[9] J.-F. Berret, N. Schonbeck, F. Gazeau, D. El Kharrat, O. Sandre, A. Vacher, and M. Airiau, J. Am. Chem. Soc. **128**, 1755 (2006).

[10] Y. R. Chemla, H. L. Grossman, Y. Poon, R. McDermott, R. Stevens, M. D. Alper, and J. Clarke, Proc. Natl. Acad. Sci. U.S.A. **97**, 14268 (2000).

[11] A. Prieto Astalan, F. Ahrentorp, C. Johansson, K. Larsson, and A. Krozer, Biosens. Bioelectron. **19**, 945 (2004).

[12] D. Eberbeck, F. Wiekhorst, U. Steinhoff, K. O. Schwarz, A. Kummrow, M. Kammel, J. Neukammer, and L. Trahms, J. Magn. Magn. Mater. **321**, 1617 (2009).

[13] F. Öisjöen, J. F. Schneiderman, M. Zaborowska, K. Shunmugavel, P. Magnelind, A. Kalabukhov, K. Petersson, A. Prieto

Astalan, C. Johansson, and D. Winkler, IEEE Trans. Appl. Supercond. **19**, 848 (2009).

[14] E. Heim, F. Ludwig, and M. Schilling, J. Magn. Magn. Mater. **321**, 1628 (2009).

[15] R. W. Chantrell and E. P. Wohlfarth, J. Magn. Magn. Mater. **40**, 1 (1983).

[16] R. W. Chantrell, N. Walmsley, J. Gore, and M. Maylin, Phys. Rev. B **63**, 024410 (2000).

[17] J. L. Dormann, F. D'Orazio, F. Lucari, E. Tronc, P. Prené, J. P. Jolivet, D. Fiorani, R. Cherkaoui, and M. Noguès, Phys. Rev. B **53**, 14291 (1996).

[18] J. Garcia-Otero, M. Porto, J. Rivas, and A. Bunde, Phys. Rev. Lett. **84**, 167 (2000).

[19] M. Hanson, C. Johansson, and S. Morup, J. Phys.: Condens. Matter **5**, 725 (1993).

[20] J.-O. Andersson, C. Djurberg, T. Jonsson, P. Svedlindh, and P. Nordblad, Phys. Rev. B **56**, 13983 (1997).

[21] M. E. J. Newman and G. T. Barkema, *Monte Carlo Methods in Statistical Physics* (Oxford University Press, New York, 1999).

[22] V. Schaller, G. Wahström, A. Sanz-Velasco, P. Enoksson, and C. Johansson, J. Magn. Magn. Mater. **321**, 1400 (2009).

[23] S. Chikazumi, *Physics of ferromagnetism* (Clarendon, Oxford, 1997).

[24] A. F. Pshenichnikov and V. V. Mekhonoshin, J. Magn. Magn. Mater. **213**, 357 (2000).

[25] R. E. Rosensweig, J. Magn. Magn. Mater. **252**, 370 (2002).

[26] D. Sellmyer and R. Skomski, *Advanced Magnetic Nanostructures* (Springer, New York, 2006).

[27] B. Gleich and J. Weizenecker, Nature (London) **435**, 1214 (2005).

[28] P. I. Nikitin, P. M. Vetoshko, and T. I. Ksenevich, J. Magn. Magn. Mater. **311**, 445 (2007).

[29] H.-J. Krause, N. Wolters, Y. Zhang, A. Offenhäusser, P. Miethe, M. H. F. Meyer, M. Hartmann, and M. Keusgen, J. Magn. Magn. Mater. **311**, 436 (2007).

[30] J. L. García-Palacios, Adv. Chem. Phys. **112**, 1 (2000).